UCRL-JC-135811
PREPRINT

High Convergence Implosion Symmetry in Cylindrical Hohlraums

O.L. Landen, P.A. Amendt, R.E. Turner, D.K. Bradley, L.J. Suter, R.J. Wallace, and B.A. Hammel

This paper was prepared for submittal to the
First International Conference on Inertial Fusion Sciences and Applications,
Bordeaux, France, September 12-19, 1999

September 1999

Lawrence Livermore National Laboratory

High Convergence Implosion Symmetry in Cylindrical Hohlraums*

O.L. Landen, P.A. Amendt, R.E. Turner, D.K. Bradley, L.J. Suter, R.J. Wallace, and B.A. Hammel

Lawrence Livermore National Laboratory, Livermore, CA 94551

Abstract

High convergence, hohlraum-driven implosions will require control of time-integrated drive asymmetries to 1% levels for ignition to succeed on the NIF. We review how core imaging provides such asymmetry measurement accuracy for the lowest order asymmetry modes, and describe recent improvements in imaging techniques that should allow detection of higher order asymmetry modes. We also present a simple analytic model explaining how the sensitivity of symmetry control to beam pointing scales as we progress from single ring per side Nova cylindrical hohlraum illumination geometries to NIF-like multiple rings per side Omega hohlraum illumination geometries and ultimately to NIF-scale hohlraums.

1. Introduction

In laser-driven hohlraums, flux asymmetries arise from the finite number of hotter laser spots and the presence of the cold laser entrance holes (LEH). For cylindrical hohlraums, these asymmetries can be decomposed into a Legendre series P_n, with P_2 usually the largest intrinsic asymmetry. The P_2 asymmetry is controlled by the pointing of the beam rings (see *Fig. 1*). For x-ray-driven ignition to succeed on the future NIF facility, P_2 flux asymmetries imposed on the imploding capsule must be maintained below 2% levels [1, 2]. The next order asymmetry, the P_4 moment, must be zeroed out to the 0.5-1% level at the capsule. This can be accomplished by using a second beam ring per side (see *Fig. 1b*), with the P_4 moment being controlled by the ring separation. Higher order asymmetry modes such as P_6 and P_8 are intrinsically smoothed out at the capsule to 1% levels, but the larger hydrodynamic instability growth of perturbations seeded by these shorter wavelength modes limits the tolerable time-integrated P_6 and P_8 to <0.5%. These conditions place stringent requirements on both measurement accuracy and symmetry control.

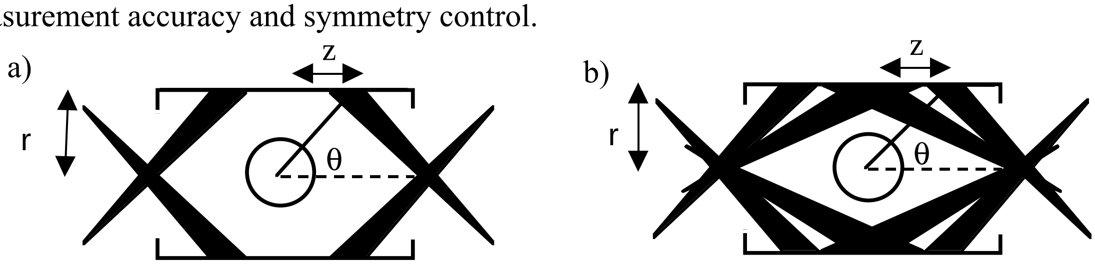

FIG. 1. Schematic cylindrical hohlraum illumination geometries used for symmetry studies. a) Nova single ring per side geometry b) Omega dual ring per side geometry with a 1:3 split in inner:outer ring energy.

2. Implosion Symmetry

In the most direct method of assessing the time-integrated asymmetries, a 500-um diameter capsule [3, 4] filled with D_2 gas and a trace of Ar gas is placed in the center of a Nova hohlraum and is imploded by x-ray drive. Following the implosion is a bright flash of x rays produced by the hot, compressed fuel and enhanced by the mid Z Ar. At that instant, we take snapshots of the core images formed by x rays viewed at $\theta = 90^{\circ}$ off the polar axis (see *Fig. 1*). The resulting images show emission that is round, oblate, or prolate, depending on the beam pointing. To a good approximation the final distortion at peak compression time is proportional to the fractional pressure asymmetry and distance travelled, multiplied by a constant close to unity:

$$a_n \approx -P_n a_0 \tag{1}$$

Dividing by the final core diameter a_f, with the convergence ratio $C_r \approx a_0/a_f$ for large C_r:

$$a_n/a_f \approx -P_n a_0/a_f \approx -P_n C_r \tag{2}$$

Eq. (2) states that the fractional distortion is proportional to the average fractional pressure asymmetry, magnified by the convergence ratio. For time-varying pressure asymmetries, a properly time-weighted flux asymmetry is required.

Typical convergence ratios for these implosions are 7 – 17, with central emitting core diameters of 20-40 μm. Given current diffraction- and noise-limited spatial resolutions of 7-10 μm, only the lowest order modes are accurately resolvable. To date, the images have been primarily analyzed for P_2 asymmetry, and historically quantified by their easily visible ellipticity, that is, the ratio of the core full width at half maximum (FWHM) at the equator at $\theta = 90°$, a, to the FWHM at the pole at $\theta = 0°$, b, where:

$$a/b = (1 + a_n/2a_f)/(1- a_n/a_f) \approx 1 + (3/2)P_n C_r \quad \text{for small values of } a_n/a_f \tag{3}$$

The final relationship in Eq. (3) assumes that P_2 is the dominant asymmetry; for example, if the P_4 and P_2 components were equal, there would be of order 50% correction in Eq. (6) in relating P_2 to a/b.

3. Pointing Sensitivity

Time-integrated control of P_2 to the 1-2% level has been demonstrated by appropriate beam pointing in single ring per side illumination for both vacuum [3, 4] and gas-filled hohlraums [5, 6], and for dual ring per side illumination [7, 8]. All campaigns used 2.1-2.5 mm-long, 0.8 mm-radius hohlraums with 0.6 mm-radius LEHs. The hohlraums were driven by 1- 2.5 ns-long, 10-20 TW, 3ω beams from the Nova and Omega lasers, and reached peak temperatures of 180-220 eV.

Based on a compilation of earlier work [1, 4], a semi-empirical formula has been derived [9, 10] for describing the time-dependent P_2 pressure asymmetry at a capsule in a cylindrical hohlraum. It is principally a function of the time-dependent angular position θ subtended by the centroid of the laser ring absorption surface at the capsule (see *Fig. 1*). Plotted as a dashed line in *Fig. 2a* is the value of P_2/P_0 at the capsule at the time of peak drive power as a function of the angular position θ of a single laser ring. We include the smoothing factor for a spherical capsule of radius r_c in a cylindrical hohlraum of typical length-to-radius r ratio = 3. We note that the node of P_2 is not at the traditional 54.7° because we have also included the effects of a non-zero unirradiated wall albedo and the presence of the lossy LEHs. Also plotted on *Fig. 2a* is the sensitivity of P_2 to beam pointing position z from the mid-plane (where $z = r\sin\theta$ by *Fig. 1*) for both single and dual ring per side illumination. The dots represent the positions of the beam rings at peak power which are typical for producing a round implosion. The P_2 sensitivity to pointing is reduced by factors of 3-5 for a dual ring geometry for the following two reasons:

1) Pointing with a single ring must be close to the P_2 node to ensure a round implosion, which is precisely where the value of P_2 is varying most rapidly.

2) The laser source power is spread roughly equally between two rings, roughly halving the sensitivity to pointing for a given ring.

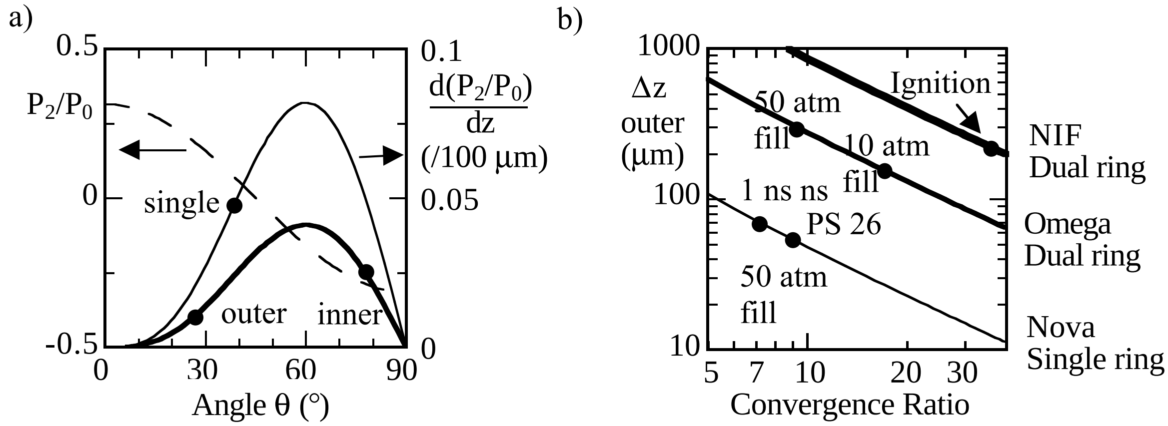

FIG. 2 a) P_2/P_0 (left-hand axis) and sensitivity of P_2/P_0 to beam ring centroid position (right-hand axis) vs. beam ring centroid angular position. b) Outer ring pointing offset for an imploded core ellipticity $\Delta(a/b) = 0.3$ as a function of convergence ratio for various hohlraum illumination geometries. Dots represent past and future implosion campaigns.

Combining the results shown in *Fig. 2a* with Eq. (3), the pointing offset required to produce a core distortion of $\Delta(a/b) = 0.3$ is plotted as a function of convergence ratio for both the single ring and outer ring of the dual ring in *Fig. 2b*. The dots represent past and future implosion campaigns; 1 ns and PS26 refer to drives produced by a 1 ns flattop pulse and a 2.2-ns-long shaped pulse with 5:1 contrast, respectively. For NIF, the sensitivity has been scaled to account for the 3.5x larger hohlraums and smaller case-to-capsule radius ratio (2.5 vs. 3). We note that this simple model reproduces the code simulated $C_r = 9$ Nova implosion [4] and $C_r = 35$ NIF ignition implosion [2] pointing sensitivities of 50 μm and 200 μm for this level of core distortion.

4. Recent Experiments

As a test of the improved symmetry and decreased sensitivity to pointing provided by these dual ring hohlraums, a series of moderate (8.5x) and high (17.5x) convergence, low adiabat, indirectly-driven implosions [9, 10] were performed at the Omega facility. The convergence ratio was varied by changing the initial fuel fill pressure from 50 atm to 10 atm D_2. Both low growth factor plain plastic and high growth factor Ge-doped plastic capsule ablators were used. Examples of 5 keV x-ray core images from moderate and high convergence implosions are shown in *Fig. 3a* and *b*, respectively. The measured and code simulated x-ray core image ellipticities which agree on average to 10% in a/b are shown in *Fig. 3c* as a function of convergence ratio. The convergence ratios (both measured and simulated) are inferred from converged fuel areal density estimates based on ratios of secondary to primary neutron yields. The agreement with simulations is especially noteworthy given that the average P_2 is being determined by the cancellation of two large P_2 components of opposite sign (see *Fig. 2a*).

Overplotted are envelope curves which encompass all the image data and represent, following Eq. (3), the expected out-of-round core distortions given a ± 2% P_2 asymmetry. It is likely that the scatter in a/b is related to ring-to-ring energy ratio variations or target imperfections and not to pointing variations by the following arguments. By *Fig. 2b*, a $\Delta(a/b)$ of 0.3 at $C_r = 17$ corresponds to a 150 μm pointing offset, much greater than the expected ring pointing accuracy of 20-30 μm [11]. By contrast, consider the variation in P_2 due to shot-to-shot absorbed energy variations in for example the inner ring. Since the inner ring P_2/P_0

contribution is 24%/2 ≈ 12% by Fig. 2a (dividing by 2 since there are two rings), an ≈ 15% variation in absorbed energy on the inner ring could lead to a 2% variation in P_2/P_0. Similarly, a barely detectable 1% variation in capsule shell thickness (0.3 μm out of 30 μm) could lead to $\Delta(a/b) > 0.3$ at these convergences. For NIF ignition, ring-to-ring absorbed energy ratios repeatable to 10% will be required, while sensitivity to absolute shell thickness variations will be less due to the 4x larger capsule dimensions.

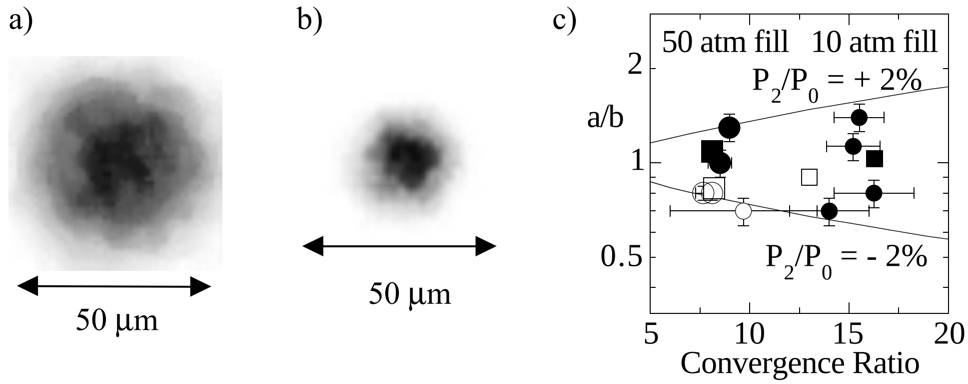

FIG. 3. a) 22x magnification 5 keV image of C_r = 9 Omega implosion. b) 13x magnification 5 keV image of C_r = 17 Omega implosion. Sizes quoted is in object plane in both cases. c) Measured and simulated core image ellipticities (a/b) as a function of convergence ratio for Ge-doped (closed circles) and undoped ablators (open circles). Overplotted is predicted ellipticities for ± 2% time-integrated P_2/P_0.

5. Implosion Symmetry Diagnosis at NIF-Scale

For inferring time-integrated symmetry from imploded core images, the accuracy according to Eq. (1) scales with initial capsule size. Hence, scaled from Nova and Omega results, NIF time-integrated accuracies for ΔP_2 of 1-2%/4 = 0.25-0.5% should be feasible. Moreover, up until recently, implosion imaging was not optimized for available detector formats. For example, a typical 12x magnification image of a 50 μm diameter imploded core only covered 1% of the detector area allocated for that particular frame. Increasing the magnification so that core image sizes at the detector plane match the cm-size detector formats should further improve accuracy and allow higher order modes to be detected. It should be noted that backlit images of low convergence surrogate spheres such as foamballs [12, 13] and thin shells [14] which nearly fully fill the detector area available have provided μm accuracy in inferring drive asymmetry induced distortions for modes at least up to P_6. The same accuracy should be attainable from high convergence imploded core images by using ultra-high (100-200X) magnification imaging with target mounted pinholes [15] (see *Fig. 4*).

Consider the multiple advantages of increasing magnification by leaving the detector position fixed while decreasing the imaging pinhole to source distance. This scenario leads to ≈ the same photon fluence at the detector while increasing the image size and hence number of photons collected. Hence, the signal-to-noise ratio (SNR) is improved both because more photons are collected per resolution element at the object, and because each image resolution element encompasses more detector resolution elements, thereby providing more averaging over detector non-uniformities. For such ultra-high magnification imaging, *Fig. 4* shows the expected scaling between Omega and NIF configurations based on debris and flux concerns. Besides the previously mentioned improved distortion measurement accuracy from using 4x larger capsules, the SNR should be even better than achieved so far at Nova and Omega for the following reasons:

1) The longer time-scales will mean that the x-ray flash from the imploded core will be further separated in time from the end of the laser drive, reducing relative background levels.
2) The higher convergence ratio implosions (30-40) possible with NIF will translate to a proportionately smaller field-of-view required for implosion imaging relative to hohlraum dimensions, further reducing contamination from laser-plasma emission.

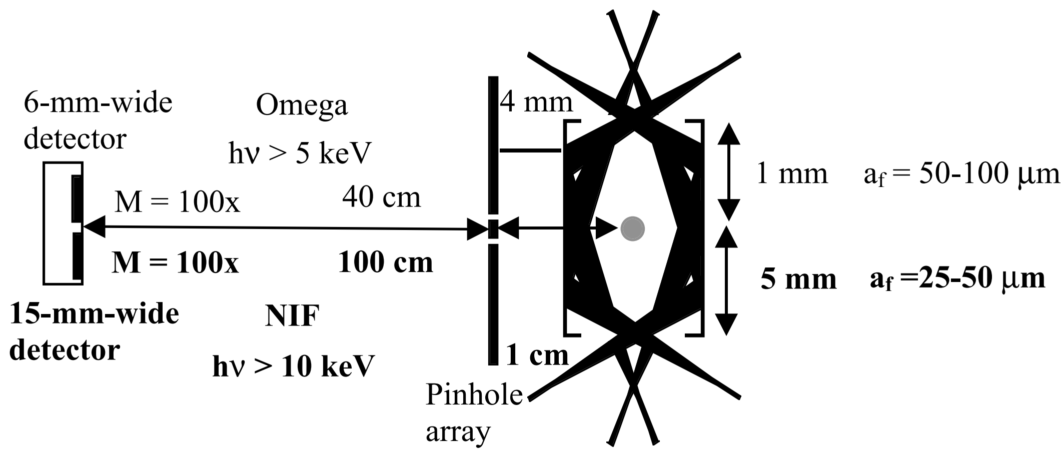

FIG. 4. Core x-ray imaging configuration using target mounted pinhole arrays for Omega/Nova and NIF-scale.

An example of a >4 keV, 5 μm-resolution, 100x magnification gated image of a 17x convergence Omega implosion is shown in *Fig. 5a*, to be compared with the 13x magnification image shown in *Fig 3b*. Both images were taken at above 4 keV by viewing through thin-wall hohlraums (4 μm of Au + 100 μm of plastic) driven by 15 kJ, 2.2 ns-long pulses at Omega. It should be noted that the 100x image in *Fig.5a* was superimposed on a background signal with 5x the average intensity of the peak core image. We note that a P_4 asymmetry is observable even at a contour surface of radius of only 5 μm. A 3.6-μm-wide line-out across the image and along the hohlraum axis is shown in *Fig. 5b*. Had this image superimposed on background been taken at the usual 12x magnification, it is doubtful a sensible image or line-out could be shown (i.e. SNR too poor) or even that the image could have been conclusively attributed as real and not an artifact of the detector without further detector flatfielding. The background can probably be reduced on future shots by increasing shielding of the hohlraum laser plasma emission.

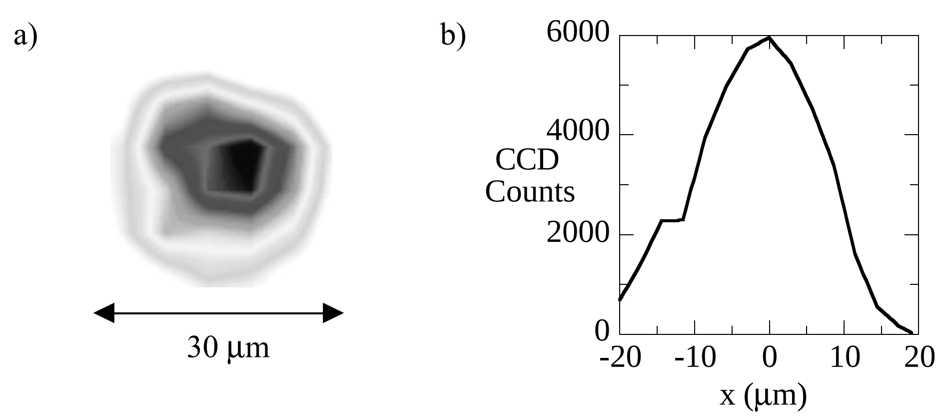

FIG. 5 a) 100x magnification 5 keV image of C_r = 17 Omega implosion. b) 3.6-μm-wide horizontal line-out showing 20 μm FWHM.

6) Summary

Core x-ray imaging of hot, converged implosions should continue to be a highly useful measure of time-integrated drive asymmetry on NIF. Recent high convergence implosions in NIF-like illumination geometries conducted at Omega have shown that code simulations and data agree on the value of the lowest order time-integrated asymmetry mode (P_2) to within 0.5% on average. Based on a simple model of the sensitivity of the P_2 asymmetry in cylindrical hohlraums to laser ring pointing and ring-to-ring energy balance, the shot-to-shot scatter in core symmetry observed is attributed to -to-ring absorbed energy variations and/or target shell thickness variations rather than to ring pointing errors. The information density on core images can be further improved by increasing magnification (from 10x to 100x levels). This should allow the presence of time-integrated higher order asymmetry modes to be inferred from such images. Future work will concentrate on improving the robustness of ultra-high magnification core imaging, through understanding and mitigating possible pinhole closure and high energy hohlraum background emission. The accuracy of inferring higher order drive asymmetry modes from real and simulated images will also be evaluated..

*This work was performed under the auspices of the US. Department of Energy by the Lawrence Livermore National Laboratory under contract No. W-7405-ENG-48.

[1] J.D. Lindl, Phys. of Plasmas **2** (1995) 3933.
[2] S.W. Haan et. al., Phys. of Plasmas **2** (1995) 2480.
[3] A.A. Hauer, et. al., Phys. of Plasmas **2** (1995) 2488.
[4] L.J. Suter, et. al., Phys. Rev. Lett. **73** (1994) 2328.
[5] N.D. Delamater, et. al., 'in press'.
[6] R.L. Kauffman, et. al., Phys. of Plasmas **5** (1998) 1927.
[7] T.J. Murphy, et. al., Phys. Rev. Lett. **82** (1998) 108.
[8]T.J. Murphy, et. al., Phys. of Plasmas **5** (1998) 1960.
[9] O.L. Landen, et. al., Phys. of Plasmas **6** (1999) 2137.
[10] O.L. Landen, et. al., Proc. Of 17th IAEA Fusion Energy Conf. (1999).
[11] J.Soures, et. al., Phys. of Plasmas **3** (1996) 2108.
[12] P.A. Amendt, et. al., Phys. of Plasmas **4** (1997) 1862.
[13] S. G. Glendinning, et. al., Rev. Sci. Instrum. **70** (1999) 536.
[14] O.L. Landen (these proceedings).
[15] J.A. Koch, et. al., Rev. Sci. Instrum. **70** (1999) 663.